A new resonance-like feature in the outer disc of the Milky Way

R. Drimmel, S. Khanna, E. d'Onghia, T. Tepper-García, J. Bland-Hawthorn, L. Chemin, V. Ripepi, M. Romero-Gómez, P. Ramos, E. Poggio, et al.

A&A 670, A10 (2023)
https://doi.org/10.1051/0004-6361/202244605

Astronomy & Astrophysics

A new resonance-like feature in the outer disc of the Milky Way

R. Drimmel[1], S. Khanna[1], E. D'Onghia[2], T. Tepper-García[3,4], J. Bland-Hawthorn[3,4], L. Chemin[5], V. Ripepi[6], M. Romero-Gómez[7,8,9], P. Ramos[7,8,9,10], E. Poggio[1,11], R. Andrae[12], R. Blomme[13], T. Cantat-Gaudin[12], A. Castro-Ginard[14], G. Clementini[15], F. Figueras[7,8,9], M. Fouesneau[12], Y. Frémat[13], A. Lobel[13], D. Marshall[16], and T. Muraveva[15]

[1] INAF – Osservatorio Astrofisico di Torino, Via Osservatorio 20, 10025 Pino Torinese, TO, Italy
e-mail: ronald.drimmel@inaf.it
[2] Department of Astronomy, University of Wisconsin-Madison, 475 North Charter Street, Madison, WI 53706, USA
[3] Sydney Institute for Astronomy, School of Physics, University of Sydney, Physics Rd, Camperdown, Sydney, NSW 2006, Australia
[4] Centre of Excellence for All Sky Astrophysics in Three Dimensions (ASTRO-3D), Stromlo, ACT 2611, Australia
[5] Centro de Astronomía – CITEVA, Universidad de Antofagasta, Avenida Angamos 601, Antofagasta 1270300, Chile
[6] INAF – Osservatorio Astronomico di Capodimonte, Via Moiariello 16, 80131 Napoli, Italy
[7] Institut de Ciències del Cosmos (ICCUB), Universitat de Barcelona (IEEC-UB), Martí i Franquès 1, 08028 Barcelona, Spain
[8] Departament de Física Quàntica i Astrofísica (FQA), Universitat de Barcelona (UB), C Martí i Franquès, 1, 08028 Barcelona, Spain
[9] Institut d'Estudis Espacials de Catalunya (IEEC), C Gran Capità, 2-4, 08034 Barcelona, Spain
[10] National Astronomical Observatory of Japan, 2 Chome-21-1 Osawa, Mitaka-shi, Tokyo 181-8588, Japan
[11] Université Côte d'Azur, Observatoire de la Côte d'Azur, CNRS, Laboratoire Lagrange, Bd de l'Observatoire, CS 34229, 06304 Nice Cedex 4, France
[12] Max Planck Institute for Astronomy, Königstuhl 17, 69117 Heidelberg, Germany
[13] Royal Observatory of Belgium, Ringlaan 3, 1180 Brussels, Belgium
[14] Leiden Observatory, Leiden University, Niels Bohrweg 2, 2333 CA Leiden, The Netherlands
[15] INAF – Osservatorio di Astrofisica e Scienza dello Spazio di Bologna, Via Piero Gobetti 93/3, 40129 Bologna, Italy
[16] IRAP, Université de Toulouse, CNRS, UPS, CNES, 9 Av. Colonel Roche, BP 44346, 31028 Toulouse Cedex 4, France

Received 26 July 2022 / Accepted 22 November 2022

ABSTRACT

Modern astrometric and spectroscopic surveys have revealed a wealth of structure in the phase space of stars in the Milky Way, with evidence of resonance features and non-equilibrium processes. Using the third *Gaia* data release, we present evidence of a new resonance-like feature in the outer disc of the Milky Way. The feature is most evident in the angular momentum distribution of the young classical Cepheids, a population for which we can derive accurate distances over much of the Galactic disc. We then searched for similar features in the outer disc using a much larger sample of red giant stars, as well as a compiled list of over 31 million stars with spectroscopic line-of-sight velocity measurements. While much less evident in these two older samples, the distribution of stars in action-configuration space suggests that resonance features are present here as well. The position of the feature in action-configuration space suggests that the new feature may be related to the Galactic bar, but other possibilities are discussed.

Key words. Galaxy: kinematics and dynamics – Galaxy: structure – Galaxy: disk – stars: variables: Cepheids

1. Introduction

The recent third public release of the *Gaia* survey (Gaia Collaboration 2016, 2022a, hereafter *Gaia* DR3) has provided the community with the largest ever homogeneous set of spectroscopic line-of-sight velocities ($V_{\rm los}$) for nearly 33 million stars in the Milky Way, supplementing the high-precision astrometry provided already in the *Gaia* Early Data Release 3 (Gaia Collaboration 2021a, hereafter *Gaia* EDR3). Using the new astrophysical parameters also provided in *Gaia* DR3, Gaia Collaboration (2022b, hereafter GD22) selected a large sample of red giant branch (RGB) stars to map the kinematics of the Galactic disc over an unprecedented volume of the Galactic disc. The most remarkable feature of these velocity maps was the clear signature of a quadrupole pattern in the Galactocentric $V_{\rm R}$ component in the inner disc (their Fig. 16). This bisymmetric feature in $V_{\rm R}$ is just the expected signature of a galactic bar with mean inward and outward motion on either side of its major axis. Even more remarkable were clear signatures of large-scale non-axisymmetry in $V_{\rm R}$ that are visible all the way out to the outer disc, at a galactocentric radius $R > 10$ kpc. For the first time, we can clearly compare the inner and outer Galaxy on the same velocity maps, and show the influence of the bar out to at least the outer Lindblad resonance (OLR), which is found to be beyond the solar circle. Specifically, GD22 inferred that the Milky Way bar has a pattern speed of $\Omega_{\rm bar} = 38.1\,{\rm km\,s^{-1}\,kpc^{-1}}$, with a corotation radius $R_{\rm CR} = 5.4$ kpc. This outcome is consistent with previous studies based on earlier *Gaia* data releases (Pérez-Villegas et al. 2017; Monari et al. 2019), confirming that the Milky Way has a long rather than a short bar, as previously thought, where the OLR was thought to coincide with the solar neighbourhood (Dehnen 2000).

It has long been known that the Galactic disc is not axisymmetric. Large-scale spectroscopic and photometric surveys, even

with sparse spatial coverage, already hinted at streaming or bulk motion in the disc, with trends in both Galactic height and radius (Widrow et al. 2012; Carlin et al. 2013; Williams et al. 2013; Bovy et al. 2015; Khanna et al. 2019a; Gaia Collaboration 2018). The first opportunity to study this in a homogeneous manner presented itself soon after the second *Gaia* data release (*Gaia* DR2), using which, Antoja et al. (2018) discovered large-scale diagonal ridges in the $V_\phi - R$ density space, which are even more striking when mapped by the galactocentric velocities, V_R and V_Z (Ramos et al. 2018; Fragkoudi et al. 2019; Khanna et al. 2019b; Laporte et al. 2019; Bernet et al. 2022; Lucchini et al. 2022). Additionally, Antoja et al. (2018) also discovered an overdensity, known commonly as the phase-spiral, in the $z - V_Z$ plane, when mapped by V_R or V_Z. This spiral pattern, thought to be a result of a perturbation to the Galactic disc, has since been dissected in the chemo-dynamic space (Bland-Hawthorn et al. 2019; Xu et al. 2020; Li 2021) in order to study its origins. With *Gaia* DR3, this feature can now be mapped over a much larger extent of the disc (Gaia Collaboration 2022c; Hunt et al. 2022).

Trick et al. (2019, 2021) and Trick (2022, hereafter T22) further explored the *Gaia* DR2 dataset in action-angle space. Actions are invariant quantities for a steady or slowly varying axisymmetric Galactic potential. Along with the total energy (E), these form a set of invariant quantities that can be used to trace phase-mixed substructure in the Galaxy (Kalnajs 1991; Ting & Rix 2019; Monari et al. 2019; Malhan et al. 2022). The radial action (J_R) is a measure of the eccentricity of a stellar orbit. The vertical action (J_Z) measures the excursion away from the Galactic plane, while J_ϕ is the z-component of the angular momentum, which can be used to infer the guiding radius of a stellar orbit. In particular, Trick et al. (2021, hereafter T21) plotted the distribution of J_R against L_Z to show large diagonal overdensities in this space. The features seen by T21 are a manifestation of the ridges discovered by Antoja et al. (2018). By considering the action-angle space, these features could be directly linked to a series of expected resonances of the Galactic bar. The continued efforts of several independent studies suggest that some features may not be entirely due to the action of the bar, but may also include spiral arm resonances or perturbations from satellite passages in the recent Milky Way history (Hunt & Bovy 2018; Hunt et al. 2019; Quillen et al. 2018; Fragkoudi et al. 2019; Trick et al. 2021; Martinez-Medina et al. 2019; Khanna et al. 2019b; Khoperskov & Gerhard 2022; Antoja et al. 2022).

The availability of 6D phase-space data for 33 million stars allows us not only to map the kinematics over a huge volume, but also to study the differences between features traced by various populations. In this contribution, we use the sample of the young Cepheids presented in GD22 to probe the disc kinematics to large distances and galactocentric radii. While the Cepheids constitute a relatively small sample, they have the advantage of having excellent relative distance errors that allow us to also accurately determine their individual velocities to large distances. In this sample, we note a resonance-like feature in their kinematics in the outer disc. We then turn to much larger samples of older stars with complete phase-space information to determine whether they also show evidence of a resonance feature in the outer disc.

The paper is organised as follows. In Sect. 2 we briefly describe the three datasets we used and our analysis methods. In Sect. 3 we present evidence for a new resonance-like feature in the outer disc, then we further discuss its relation to known resonance features in Sect. 4. We summarise our findings in Sect. 5.

2. Data and methods

2.1. Dataset

We restrict our analysis to three data subsets constructed primarily using *Gaia* DR3. We select both young and old stellar populations to illustrate the similarities and differences in their kinematics.

Cepheids. To trace the young population, we adopted the sample of classical Cepheids published by GD22. This consists of 1948 stars with estimated ages younger than 200 Myr and that have spectroscopic line-of-sight velocities, and their distances are estimated based on the period-Wesenheit-metallicity relation (Ripepi et al. 2019, 2022a). The relative distance error of this sample is less than 6.25% for 90% of this sample. The precision in the distances means that the uncertainties in the velocities perpendicular to the line of sight, derived from the proper motions and distances, are less than $10\,\mathrm{km\,s^{-1}}$ for 90% of our sample to a distance of 6 kpc, while the median uncertainty at this distance is less than $5\,\mathrm{km\,s^{-1}}$. Meanwhile, the median uncertainty in the spectroscopic line-of-sight velocities remains well below $5\,\mathrm{km\,s^{-1}}$ at all distances. The resulting uncertainties in the galactocentric azimuthal velocity are less than $10\,\mathrm{km\,s^{-1}}$ for 90% of our sample to a distance of at least 9 kpc from the Sun.

Red giant branch (RGB) sample. To trace the older population we adopted the exact same sample of nearly five million red giants that was used by GD22. The full details of the sample selection can be found in their paper, but it is essentially based on the position in the Kiel diagram of sources that are provided with stellar atmospheric parameters in *Gaia* DR3. The distances for this sample are taken from the photogeo distance catalogue of Bailer-Jones et al. (2021), and as in GD22, we restricted our sample to within 1 kpc of the Galactic plane.

Radial velocity (RV) sample. Finally, in order to construct the largest possible sample with full velocity information, we followed the scheme laid out in Khanna et al. (2022). We began by selecting all sources in *Gaia* DR3 with a valid `radial_velocity`. The recommended correction to the `radial_velocity_error` for these stars was then applied following Babusiaux et al. (2022). We supplemented this sample with publicly available V_{los} measurements from the following spectroscopic surveys: the LAMOST[1] DR7 low-resolution (LR; Cui et al. 2012) and medium-resolution (MR; Liu et al. 2020) surveys, RAVE[2] DR6 (Steinmetz et al. 2020), GALAH[3] DR3 (Buder et al. 2021), and APOGEE[4] DR17 (Abdurro'uf et al. 2022). To the LAMOST LR sample, we applied a $+7.76\,\mathrm{km\,s^{-1}}$ offset as recommended by their release note[5]. For stars without a *Gaia* DR3 V_{los}, we assigned velocities in the following order: GALAH, APOGEE, RAVE, and LAMOST. This is in accordance with the typical V_{los} uncertainty in these surveys. We again used the photogeo distances from Bailer-Jones et al. (2021) for this sample, but restricted to high-quality distances, requiring

$$\frac{0.5 \times (r\_\mathrm{hi\_photogeo} - r\_\mathrm{lo\_photogeo})}{r\_\mathrm{med\_photogeo}} < 0.2. \quad (1)$$

With this cut, we removed about 1.5 million stars from the entire sample. While the selection process for the RGB sample

[1] Large Sky Area Multi-Object Fiber Spectroscopic Telescope.
[2] RAdial Velocity Experiment.
[3] GALactic Archaeology with HERMES.
[4] Apache Point Observatory Galactic Evolution Experiment.
[5] https://dr7.lamost.org/v2.0/doc/release-note

Table 1. Number of stars contributed by the individual surveys to our extended RV sample.

Survey	N	N ($\|z\| < 1$ kpc)
Gaia DR3	32 390 397	30 142 671
LAMOST LR	1 876 313	1 295 921
LAMOST MR	29 168	24 977
APOGEE	85 994	72 086
GALAH	17 673	15 198
RAVE	7556	7239
Total	34 407 101	31 558 092

Notes. All stars here satisfy the distance uncertainty condition in Eq. (1).

was more sophisticated, applying a distance cut as above is one way in which we can restrict to a radial velocity sample with trustworthy distances. Lastly, just as for our RGB sample, we restricted to within 1 kpc of the Galactic plane, resulting in a total of 31 558 092 stars in our final RV sample. In Table 1 we list the contribution from individual surveys that satisfy the distance quality as well as the $|z|$ selection.

2.2. Action estimation

In general, actions can be computed analytically only for potentials for which the variables can be separated, in order to solve the Hamilton-Jacobi equation (Sanders & Binney 2016). Spherical and Stäckel potentials (de Zeeuw 1985) are examples where this is possible. For more general axisymmetric potentials, Binney (2012) developed a method in which the gravitational potential is assumed to be similar to a Stäckel potential. This so-called Stäckel-fudge method is implemented in the AGAMA code (Vasiliev 2019) to calculate the classical axisymmetric actions $J = (J_R, J_\phi, J_Z)$ mentioned in the Introduction. The actions estimated in this way remain conserved over time and serve as true integrals of motion only in an axisymmetric potential. For a more realistic Galactic potential (e.g. the Milky Way), with clear non-axisymmetric features such as a bar and spiral arms, this is not the case. However, combining the Stäckel-fudge method with an axisymmetric potential that is well fitted to observed data still allows us to estimate the instantaneous axisymmetric actions and to extract the main features and substructure of the underlying kinematics in the Galaxy. Essentially, any substructure that appears in this action space is likely due to non-axisymmetric or time-varying components of the gravitational potential, whether the actions are accurate or not. We used the AGAMA code to compute the instantaneous set of actions, $J = (J_R, J_\phi, J_Z)$, in three different axisymmetric potentials: (a) Cautun20, (b) McMillan17, and (c) MWPotential2014 (Cautun et al. 2020; McMillan 2017; Bovy 2015, respectively).

2.3. Coordinate transformations

We followed the scheme used in GD22 to transform sky coordinates, proper motions, and distances to galactocentric positions and velocities. That is, to compute the azimuthal components of the galactocentric velocity of the Sun, we used the precise measurement by Reid & Brunthaler (2020) of the proper motion of Sgr A*, that is, $(\mu_l, \mu_b) = (-6.411 \pm 0.008, -0.219 \pm 0.007)$ mas yr^{-1}. The most recent measurement of the orbit of star S2 around the supermassive black hole of the Milky Way from the ESO Gravity project yields both a very precise distance to the Galactic centre, $R_\odot = 8277 \pm 9$ (stat.) ± 30 (sys.) pc, and the line-of-sight velocity towards Sgr A* (GRAVITY Collaboration 2021). Assuming that Sgr A* is stationary with respect to the Galactic centre, this gives

$$\boldsymbol{v}_\odot = \begin{pmatrix} 9.3 \pm 1.3 \\ 251.5 \pm 1.0 \\ 8.59 \pm 0.28 \end{pmatrix} \mathrm{km\,s^{-1}}, \quad (2)$$

for the solar velocity with respect to the Galactic centre in galactocentric Cartesian coordinates. The height of the Sun above the Galactic plane is assumed to be 0 and the X axis is taken toward the Galactic centre. In galactocentric cylindrical coordinates, our velocities are (V_R, V_ϕ, V_Z), with V_ϕ taken positive in the direction of Galactic rotation (i.e. clockwise).

3. Signature of an outer resonance

3.1. Kinematics of the Cepheids

We here considered the kinematics of the young Cepheids from GD22. Plotting their azimuthal velocity with respect to the galactocentric radius (i.e. the rotation curve), we note a gap in the azimuthal velocity distribution at approximately $R = 13$ kpc (see Fig. 1a). This gap has a negative slope with respect to R at about 12 kpc to 14 kpc. However, plotting the angular momentum of the Cepheids (Fig. 1b) shows that this gap is apparently at a fixed value of $L_Z (= V_\phi R)$. In Fig. 2 we show the 1D distribution in L_Z for the Cepheid sample, where the gap can quite clearly be identified in this space. To estimate the precise location and its width, we performed a kernel density estimate (KDE) using the SKLEARN package (Pedregosa et al. 2011). We used a Gaussian kernel, setting the bandwidth following Scott (1992), and performed the KDE on 1000 bootstrapped samples. In Fig. 2 this is shown as the set of smoothed histograms in the background (orange). For each of the 1000 samples, we estimated the minimum between $2800 < L_z < 3100$. We find that the dip in the Cepheid L_Z distribution occurs at $L_Z = 2950 \pm 46\,\mathrm{km\,s^{-1}}$ kpc. Because this gap is well defined and at a fixed value of angular momentum, a conserved quantity, it has the characteristic of being a resonance feature. However, as we discuss further in Sect. 5, this interpretation is problematic.

We also note that this gap coincides with an apparent bump in the rotation curve of the Cepheids derived from radially binning their azimuthal velocities (see Fig. 1a). However, this bump is just an artefact of the noted gap itself. We therefore locate the radius of this resonance-like feature using the L_Z distribution instead, which is very well described by a simple linear fit. We find $L_Z = 231.4\,R + 9.65\,\mathrm{km\,s^{-1}}$ kpc, with a correlation of 0.87. We note that the intercept is insignificantly small. Dropping this last term, we can therefore adopt $R_g \equiv L_Z/231.4$ kpc as the guiding radius for each star. The location of this feature is then taken as the guiding radius for $L_Z = 2950\,\mathrm{km\,s^{-1}}$ kpc, that is, at $R_g = 12.75$ kpc. In Sect. 4 below, we discuss the location of this feature and its relation to the known resonances of the bar.

As L_Z correlates well with R, it might be wondered whether a gap in the radial distribution might cause the feature seen at $L_Z = 2950\,\mathrm{km\,s^{-1}}$ kpc. The feature is indeed found in a restricted range of radii, as the L_Z distribution (Fig. 1a) has a finite width in radius. However, in this same radial range lie Cepheids with both lower and higher values of L_Z. The distribution of L_Z is nevertheless modulated to some degree by the spatial distribution of Cepheids in the Galactic plane. Poggio et al. (2021) and GD22

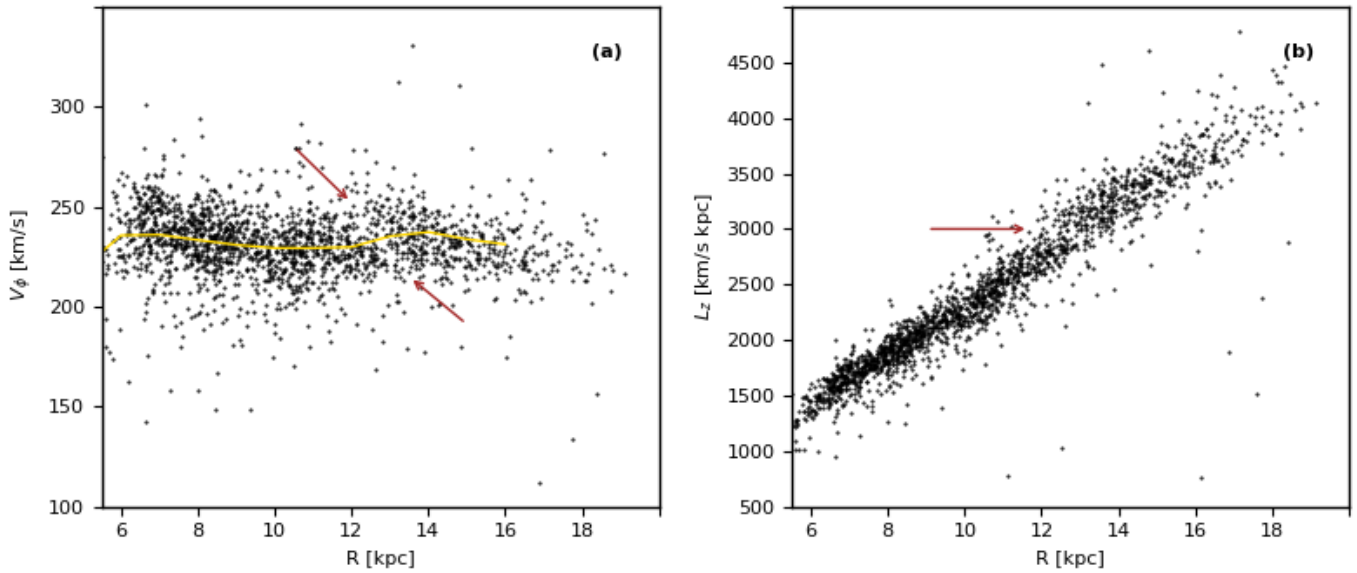

Fig. 1. Observed azimuthal velocities (*panel a*) and specific angular momentum (*panel b*) of the young Cepheids. The yellow curve in panel a traces the median rotation curve for the sample. The arrows in both panels indicate the apparent gap in the distribution and the location of a new resonance-like feature around $L_Z \sim 3000\,\mathrm{km\,s^{-1}}$ kpc.

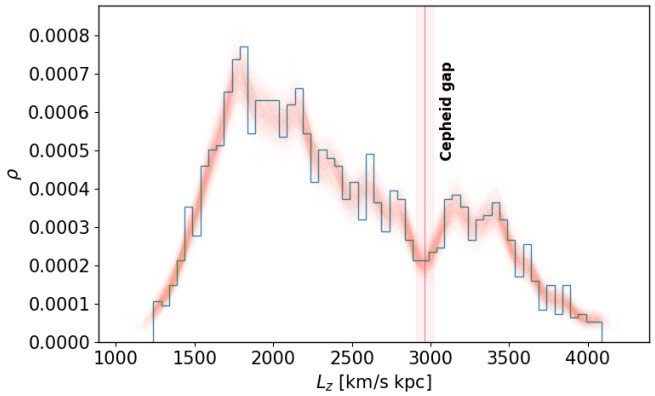

Fig. 2. Distribution of the z-component of angular momentum (L_Z) for the Cepheid sample, shown as a solid blue line. In the background we overplot the KDE estimates of 1000 bootstrapped samples in orange. The solid orange vertical line (and the shaded region) marks the position of the dip in the L_Z distribution at $2950 \pm 46\,\mathrm{km\,s^{-1}}$ kpc. This corresponds to the gap marked in Fig. 1.

pointed out that the Cepheids in the outer disc trace an outer spiral nicely that is seen in HI, as modelled by Levine et al. (2006). However, this arm is mainly in the third quadrant, but we also see the gap in the L_Z distribution for the Cepheids in the first and second quadrants.

We also checked possible selection effects that might cause this gap. We can exclude extinction effects, as Cepheids with a given L_Z are not restricted to a small area on the sky, but span a wide range of Galactic azimuth. Moreover, extinction would indiscriminately remove Cepheids for a wide range of L_Z. Compared to independent high-fidelity Cepheid catalogues in the literature, it is estimated that our *Gaia* DR3 sample of Cepheids is approximately complete to 90% (Ripepi et al. 2022b). This likely varies depending on the number of epochs available for characterising the variability, which is determined by the *Gaia* scanning law. However, this will only introduce an on-sky directional dependence, which, like extinction, will not selectively remove Cepheids at a particular distance or angular momentum.

3.2. Kinematics of the RGB and RV samples

The Cepheid sample has revealed an interesting feature in the L_Z distribution in Fig. 2, suggesting the presence of a resonance. We now study the RV and RGB datasets to gain a manifold increase in density (from 1000 s to millions of stars), allowing us to explore the distribution in action space where we expect to see the signature of the resonances more clearly. In Fig. 3 we plot the distribution of the two datasets in the ($\sqrt{J_\mathrm{R}}, L_Z$) plane for the four different axisymmetric potentials listed in Sect. 2. We normalised both axes by the z-component of angular momentum at the Sun, $L_{Z,\odot} = 2081.6\,\mathrm{km\,s^{-1}}$ kpc. We recovered the large-scale diagonal features (ridges) seen in this space by T21. (Unlike T21, we chose to present our results using $\sqrt{J_\mathrm{R}}$ and not J_R itself, as it enhances the features slightly). The RV sample, being dominated by nearby bright stars, shows a high concentration near $L_{Z,\odot}$. The RGB distribution is comparatively diffuse while retaining most of the ridge features. We also note that while there are subtle differences between the individual potentials, they map similar features overall. In this regard, the MWPotential2014 seems to be least consistent with the other two potentials. This might be due to the difference in the circular velocity normalisation between the potentials. In particular, a group of stars that rotates close to the circular velocity of a chosen potential,will be on nearly circular orbits and thus have lower J_R. Because the circular velocity in the MWPotential2014 is about $220\,\mathrm{km\,s^{-1}}$ while in the other two it is about $230\,\mathrm{km\,s^{-1}}$, this would explain the vertical shift to lower J_R in MWPotential2014.

Compared to T21, we have the benefit of adding more data in the outer disc thanks to *Gaia* DR3. Keeping Fig. 2 in mind, we are interested in probing the region around $L_Z = 2950\,\mathrm{km\,s^{-1}}$ kpc (or $\sim 1.42\,L_{Z,\odot}$). However, it is clear from Fig. 3 that even with the added coverage, the density in action space falls off sharply beyond this L_Z value. Nevertheless, no clear gap in the distribution is seen. Thus, we again followed T21 and show in Fig. 4 the same distribution in the ($\sqrt{J_\mathrm{R}}, L_Z$) plane, but now mapped

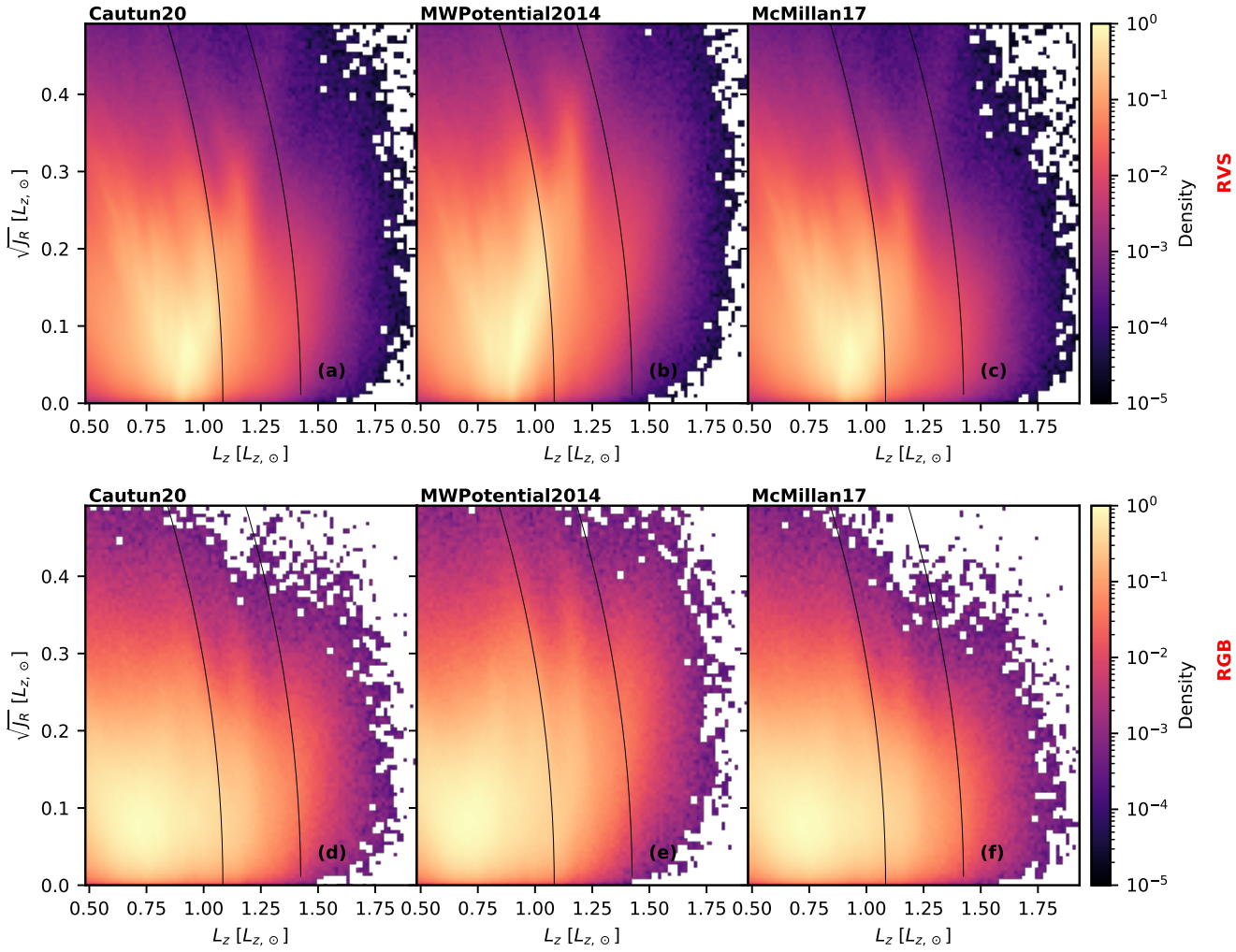

Fig. 3. Distribution in ($\sqrt{J_R}, L_Z$) plane for the RV (*upper panels*) and the RGB (*lower panels*) samples, computed using AGAMA for four different gravitational potentials. Both datasets show diagonal ridges, but the RGB sample extends farther into the outer disc. Beyond 1.42 $L_{Z,\odot}$ the density falls off sharply, which makes it harder to distinguish features.The black curves mark the expected OLR of the bar at 1.08 $L_{Z,\odot}$ and the Cepheid gap at 1.42 $L_{Z,\odot}$.

by $N(V_R < 0)/N_{tot}$, that is, the fraction of sources moving in towards the Galactic centre. This has two immediate effects: first, it makes the diagonal features stand out dramatically, and second, we are now able to observe features for the entire extent of our datasets. Our Fig. 4 can be directly compared to Figs. 1, 11 and 12 in T21, who were limited in coverage out to about $L_Z/L_{Z,\odot} = 1.4$. For their analysis, T21 used the galpy (Bovy 2015) code, using the MWPotential2014 to compute the actions, that is, it is comparable to Fig. 4c. T21 and T22 also showed that the ridges in action space can be roughly traced with lines with a negative slope of about −1 in (J_R, L_Z), at different locations in L_Z, corresponding to the various resonances. The purpose of including this slope is only to serve as a guide to the reader.

In Fig. 3 we plot two such lines (curves in $\sqrt{J_R}, L_Z$). The first line is at the expected location of the OLR of the bar, based on GD22, around $R_g = 9.7$ kpc, or at 1.08 $L_{Z,\odot}$ (231.4 × $R_g/L_{Z,\odot}$). As Fig. 5 shows, however, an uncertainty is associated with the location of the OLR (shaded region), and could be as large as $R_g = 10.2$. Here, we chose the median value of $R_g = 9.7$ kpc, but a higher value, as well as a different choice of the circular velocity at the Sun, will shift the expected location of the resonance. The second curve is at the Cepheid gap presented in Fig. 2 at 1.42 $L_{Z,\odot}$. The OLR ridge indeed seems to be traced well with the first curve, but we note that the ridge has a width that is also expected (see e.g. Binney 2020). The second curve, corresponding to the new feature, is harder to link to any ridge. Similarly, we also overplot the two curves in Fig. 4, which maps $N(V_R < 0)/N_{tot}$. In each potential, the OLR curve seems to mark a boundary between inward and outward systematic motions. This is consistent in the RV and the RGB samples (but as before, more diffuse in the latter).

The classically expected orbital behaviour around the OLR (Weinberg 1994; Dehnen 2000; Sellwood 2010) was illustrated in action space by the test particle simulations of T21 and T22. In particular, because the Galactic bar leads the Sun by about 20 degrees, the stars inside the OLR curve (lower L_Z) are expected to move outwards (red), while those outside the OLR curve (higher L_Z) would be expected to move inwards (blue). However, the observed behaviour is opposite to this expectation. This was also remarked upon by T21 and T22. In particular, they showed in their analysis using angle space (instead of actions) that a pattern speed close to our adopted value from GD22 seems to be the most favourable candidate to explain the expected velocity distribution around the OLR, although it was not clear why the

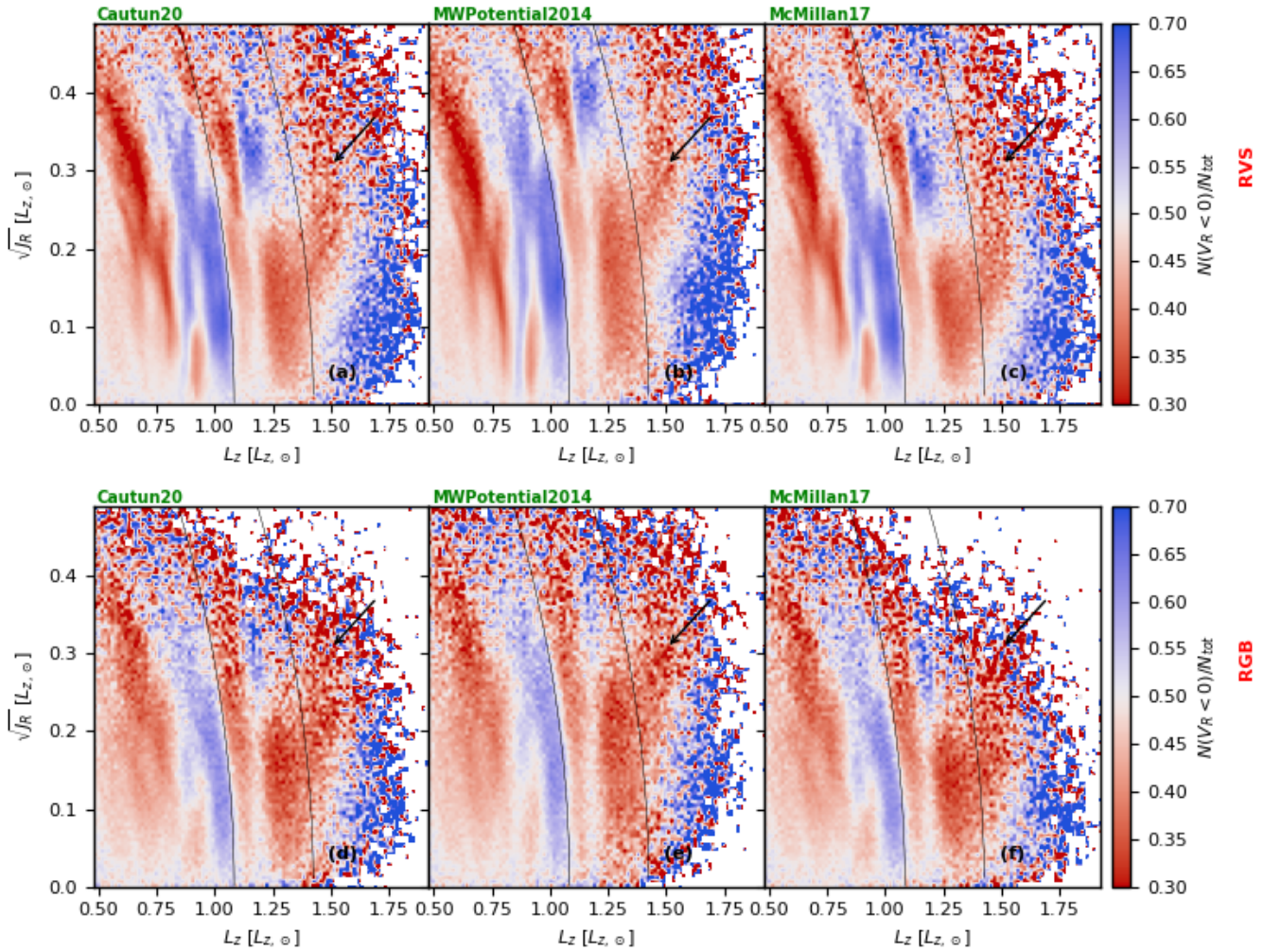

Fig. 4. Distribution in the ($\sqrt{J_R}, L_Z$) plane for the RV (*upper panels*) and the RGB (*lower panels*) samples, computed using AGAMA for four different potentials. Here we colour-code the distribution by the fraction of stars moving inward ($V_R < 0$). The black curves mark the expected OLR of the bar at 1.08 $L_{Z,\odot}$ and the Cepheid gap at 1.42 $L_{Z,\odot}$. The diagonal ridges are much clearer in this space than in Fig. 3. We report a previously unseen new overdensity of outward-moving stars just beyond the Cepheid gap. This is marked by black arrows.

orientation was flipped in action space. Notwithstanding this open question regarding the correct orientation of the red-blue feature at resonances, we continue to refer to it as the OLR because our predicted location for the OLR marks a boundary in this space.

The location of the second curve is quite interesting for two reasons. First, inwards of the second curve is the dataset that was mapped by T21. In particular, they were the first to show the ridge just inside of this curve. We are now able to present a new feature of net positive radial motions just outside this second curve (marked by black arrows). That is, we find a clump of outward-moving stars with high radial action ($\sqrt{J_R} > 0.15$ in McMillan17), although as before, we note subtle differences between the individual potentials.

Our coverage extends out to almost $L_Z/L_{Z,\odot} = 2$. In the region beyond $L_Z/L_{Z,\odot} > 1.7$, there is a notable feature of negative radial motions (in blue) in Fig. 4. This might be another interesting feature worth exploring, as we see it regardless of which distance estimator is used, those from Bailer-Jones et al. (2021), or inverse parallax (not shown here). We recall, however, the possibility of artefacts at the edge of our data coverage (see also GD22).

4. Discussion

4.1. Possible 1:1 resonance with the bar

As mentioned above, because we observe a gap in the azimuthal velocity radial distribution that is at a fixed value of L_Z, a conserved quantity for an axisymmetric potential, this feature might be due to a resonance. We now discuss the position of this feature with respect to the other known resonances in the disc. Figure 5 shows the angular velocity of the RGB and OB stars and the corotation and the OLR of the bar, according to GD22. We note that the position of the resonance feature at $R_g = 12.7$ kpc is near to the expected position of the 1:1 resonance of the bar.

The clarity and sharpness of this outer feature in L_Z–R space motivate us to hypothesise that this is a 1:1 resonance feature, and to derive the pattern speed of the bar accordingly. We used the angular velocity of the Cepheids rather than that of the RGB stars as done in GD22, as it will be closer to the actual circular velocity of the disc because of the youth and low velocity dispersion of this sample. In Fig. 6 we show the resulting $\Omega(R_g)$ curve for the Cepheids. From Binney & Tremaine (2008, Eqs. (3)–(59)),

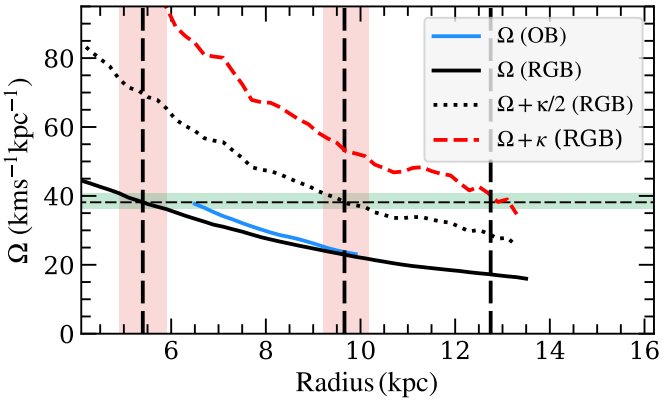

Fig. 5. Angular velocity of the RGB (solid black curve) and OB stars (solid blue curve). The dashed vertical lines mark the estimated position of corotation (5.4 kpc) and the OLR (9.7 kpc), as estimated in GD22, and the new resonance-like feature at 12.75 kpc. The thin horizontal dashed line indicates the pattern speed inferred from the corotation radius. We note that the radius of the new resonance-like feature is quite close to the radius where $(\Omega + \kappa)$ is equal to the pattern speed of the bar, that is, approximately at the expected radius of the 1:1 resonance of the bar.

the epicyclic frequency in the epicyclic approximation is

$$\kappa^2(R) = \left(R\frac{\mathrm{d}\Omega^2}{\mathrm{d}R} + 4\Omega^2 \right)_{R_\mathrm{g}} . \tag{3}$$

Taking $\Omega^2 = V_\phi^2/R^2 = L_Z^2/R^4$ and $L_Z(R_\mathrm{g}) = 231.4\,R_\mathrm{g}$ (see Sect. 3.1), we find $\Omega(R_\mathrm{g}) = 231.4/R_\mathrm{g}$ for the angular velocity of the Cepheids. The epicyclic frequency is then $\kappa(R_\mathrm{g}) = \sqrt{2}\cdot 231.4/R_\mathrm{g}$. Assuming the 1:1 resonance is at $R_\mathrm{g} = 12.75$ kpc, we find a bar pattern speed of $43.5\,\mathrm{km\,s^{-1}\,kpc^{-1}}$, with the 2:1 OLR and corotation at 9.1 kpc and 5.3 kpc, respectively. This corotation radius agrees well with that of GD22, while the radius of the OLR is about half a kiloparsec away from that estimated using the RGBs.

We have only discussed the kinematics of the Cepheids associated with their azimuthal velocities so far. However, it is worth noting what is seen in their other two velocity components with respect to galactocentric radius and this new resonance feature. Figure 7 again shows V_ϕ with respect to R, but with the V_Z and V_R velocities indicated in colour in the upper and lower panels. We also show the constant L_Z curves for the 1:1 and 2:1 (OLR) resonances, taking L_Z of the OLR to be at $R_\mathrm{g} = 9.7$ kpc, that is, $L_Z = 2244.6\,\mathrm{km\,s^{-1}}$ kpc. Since these plots integrate over a wide range in ϕ, we might not expect any clear pattern, but in the outer disc, the $L_Z = 2950\,\mathrm{km\,s^{-1}}$ kpc of the 1:1 resonance marks a clear boundary for a change in V_R and V_Z. That we also see systematic positive V_Z velocities in the part of the outer disc that we are sampling is to be expected: This is just the warp signature that has already been noted (Poggio et al. 2018). It is not expected, however, that the $L_Z = 2950\,\mathrm{km\,s^{-1}}$ kpc boundary would so clearly mark the onset of these vertical motions.

For comparison, Fig. 8 shows the RGB sample in the V_ϕ–R space, colour-coded by density, the median V_R, and the median V_Z velocities. The same plots for the full RVS (not shown) are very similar. The much larger number of stars in this sample again allows us to more clearly identify features, for instance those correlated with the OLR. With respect to V_Z, we see a similar pattern of systematic positive (upward) velocities in the outer disc, but with a clear difference with respect to the Cepheids in that the $L_Z = 2950\,\mathrm{km\,s^{-1}}$ kpc boundary does not indicate where

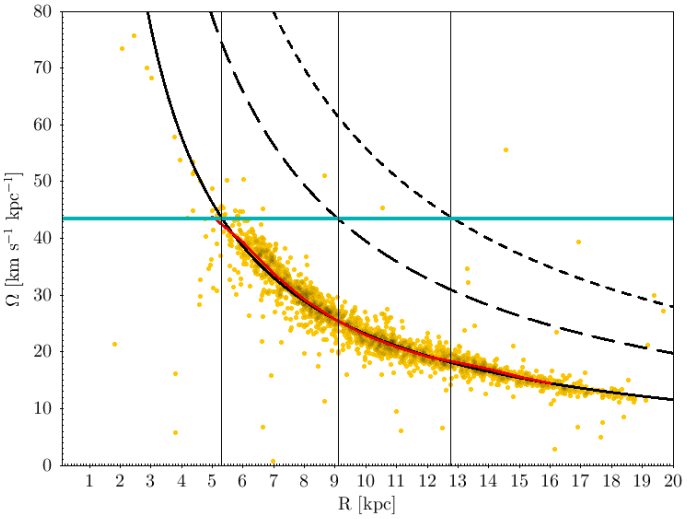

Fig. 6. Angular velocity of the Cepheids, using $\Omega(R) = L_Z(R = R_\mathrm{g})/R^2 = 231.4/R$ (solid black curve), with the angular velocity of the individual Cepheids as yellow points. The overplotted red curve is the angular velocity that would result when the Cepheid rotation curve from GD22 is used. Dashed curves are $\Omega + \kappa/2$ (long dash) and $\Omega + \kappa$ (short dash). The rightmost vertical line is at $R = 12.75$ kpc, the position of the new resonance-like feature, and the horizontal turquoise line is the resulting estimated pattern speed of the bar, assuming this feature to be the 1:1 bar resonance. The other vertical lines mark the resulting positions for corotation and the OLR.

these vertical motions begin. In any case, that curves of constant L_Z in the V_ϕ–R plane mark the boundary of the onset of systematic vertical motions suggests that the in-plane (epicyclic) and vertical motions are coupled in the outer disc, similar to what would be expected from the perturbation from a passing satellite. Alternatively, the vertical motion may be simply determined by the guiding radius of the star, for which L_Z serves as a proxy.

4.2. Comparison to previous studies

The outer disc of the Milky Way is an interesting laboratory for exploring the dynamics and past history of the Galaxy. Due to the lower gravitational potential, imprints of perturbations in this region are long lived, making these still observable today. Over the years, surveys using a variety of kinematic tracers have shown that the outer disc is corrugated and flares with increasing R (Yanny & Gardner 2013; Xu et al. 2015; Thomas et al. 2019; Bland-Hawthorn et al. 2019; Mackereth et al. 2019). Using the most recent astrometric data from *Gaia* EDR3, Gaia Collaboration (2021b, hereafter AC21) analysed the kinematics of stars in the Galactic anticentre region ($170° < l < 190°$). This window is narrow enough to assume that the line-of-sight velocity is zero, to a good approximation. This allowed AC21 to study the kinematics of a very large sample of stars in the outer disc lacking spectroscopic line-of-sight velocities, and to discover that the velocity distribution is bimodal in this region. More recently, McMillan et al. (2022, hereafter MC22) extended this analysis to a much wider range ($130° < l < 230°$), thus vastly increasing the number density of sources and allowing a study of the variation of this bimodality with respect to galactocentric azimuth. Together, these works showed that in the $1.3\,L_{Z,\odot}$–$1.35\,L_{Z,\odot}$ region, the V_Z–L_Z space breaks sharply, and that the strength of the feature varies over galactic longitude.

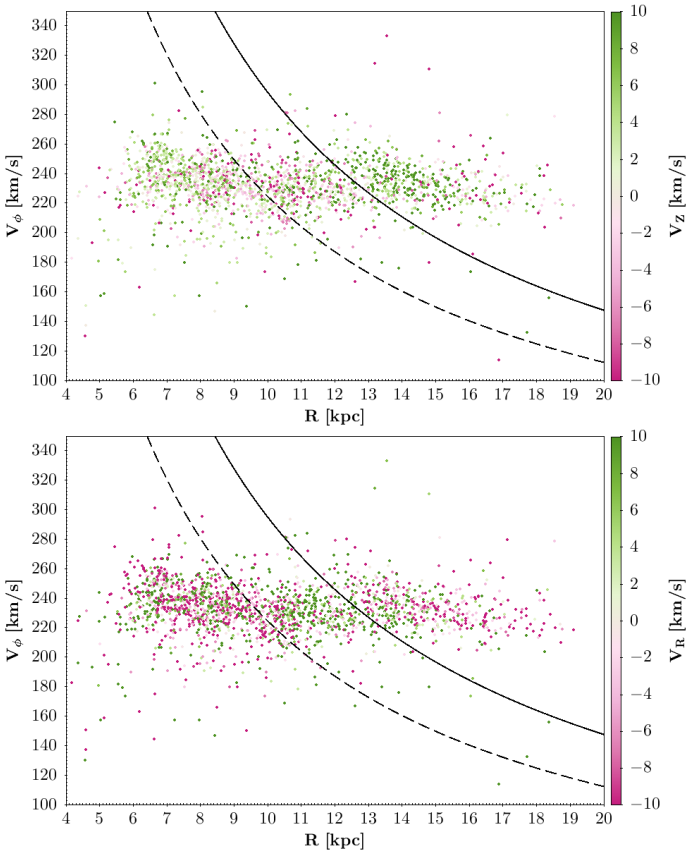

Fig. 7. Observed azimuthal velocities of the young Cepheids, with the points coloured with respect to their galactocentric vertical (upper plot) and radial velocities. Solid and dashed curves mark lines of constant L_Z of the 1:1 and 2:1 OLR, respectively.

In Fig. 9 we show our RV and RGB populations in the V_z–L_z plane, the same as were studied by AC21 and MC22. We used the new line-of-sight velocities in *Gaia* DR3, however. We divided the sample into three bins of 30° width in the azimuth, tracing either side of the anticentre. All three panels show that with an increase in R, the vertical velocity is fairly flat out to ∼1.1 $L_{Z,\odot}$. Beyond this guiding radius, the distribution appears bumpy and disturbed farther out. The middle panels in Fig. 9 are centred about the Galactic anticentre. This coverage overlaps with that of AC21. It is not surprising then that we also see a clear break in the velocity distribution around ∼1.3 $L_{Z,\odot}$. This feature has a clear dependence on azimuth, again similar to what MC22 demonstrated. We note that the position of the break seen here is just at a slightly lower L_Z compared to AC21 and MC22, but this is due to the wider azimuthal bin used here. In each of the panels, we overplot three vertical lines of interest. The two dotted black lines in each panel are the expected 2:1 OLR (∼1.08 $L_{Z,\odot}$) and the 1:1 (∼1.42 $L_{Z,\odot}$) resonance lines for the pattern speed of the GD22 bar. Additionally, we also overplot the location of the bimodality as observed by us at ∼1.3 $L_{Z,\odot}$ in green. The velocity distribution in Fig. 9 and the overplotted lines of interest suggest that the Cepheid L_Z gap we observe in Fig. 2 is distinct from the bimodality break discovered by AC21 and MC22. Lastly, we also note a bump-like feature in V_z–L_z, both around the location of the Cepheid gap at ∼1.42 $L_{Z,\odot}$ and in the acceptable range for the OLR (∼1.08 $L_{Z,\odot}$–1.17 $L_{Z,\odot}$). We do not draw any conclusions from this. It is likely a mere coincidence, although investigating the signature of vertical oscillations around resonances is interesting in itself.

5. Conclusions

As the quadrupole moment of the bar potential falls off as R^{-3} outside the bar (Sect. 2.4 Binney & Tremaine 2008; Weinberg 1994), it is not expected that the bar would have much influence beyond its OLR. We cannot be sure that we see a corresponding resonance signature in the RGB and RV samples, and if we do see one, it is very weak. However, we note that Trick et al. (2021) mentioned the possible detection of a weak signature at the 1:1 resonance already in *Gaia* DR2 data, based on comparisons with simulations of test particles responding to a barred potential. Our Cepheid sample, however, has important differences with respect to the older RGB and RV samples. First, it is dynamically very young at this point in the disc: These stars have not yet completed a single orbit about the Galactic centre. With ages younger than 200 Myr, in the outer disc they should be considered as tracers of the gas from which they were born, as they have not had time to respond to a resonance since their birth. However, we do not expect the 1:1 resonance to manifest itself in the gas either: Unlike the Lindblad resonances and corotation in the weak bar regime (see Sect. 3.3 of Binney & Tremaine 2008), we do not expect to see a change in the orientation of closed orbits at this resonance. We also investigated the gas response in the outer disc to a barred potential by studying the gas dynamics in already extant simulations of the Milky Way in more detail (see Appendix A). No clear resonance-like feature is manifested at the position of the 1:1 resonance here either. More appropriate comparisons with simulations of a young stellar population, along the lines of Pettitt et al. (2020), should be performed in the future.

Their excellent distances and intrinsic low velocity dispersion are important characteristics of this sample that help us to see what would otherwise be subtle features in their kinematics. The quality of their distances not only assists in accurately assigning a galactocentric radius to each star, but also in deriving an accurate velocity perpendicular to their line of sight. Their low velocity dispersion allows us to see narrow features that would otherwise be erased over time in a sample with a higher velocity dispersion. However, if we are detecting a resonance feature, the question remains as to why we do not see a similar feature at the OLR of the bar.

An alternative explanation is that we do not see a resonance feature from the bar, but instead a resonance from the spiral arms. For a bar with a pattern speed of ∼40 km s^{-1} kpc^{-1}, the spiral arms that develop at the edge of the bar have a pattern speed of 30 km s^{-1} kpc^{-1}, and their OLR is between 11 and 13 kpc (see Fig. 11 of models of a barred Milky Way in D'Onghia & Aguerri 2020). If this new feature is the OLR of the spiral arms, a pattern speed of 31 km s^{-1} kpc^{-1} is deduced, which would place the corotation of the spiral arms near the solar circle. However, if the spiral structure that propagates outwards in the disc has a lower pattern speed (∼20 km s^{-1} kpc^{-1}), then our detected feature may be a response to corotation. Barros et al. (2013) argued that a resonance feature at the corotation of the spiral arms should indeed be expected, although they reported such a feature close to the solar circle, at R ∼ 9 kpc. In either case, it would indicate that we have identified a spiral arm resonance that overlaps with a bar resonance.

Recent efforts to deduce a spiral arm pattern speed in the Milky Way have yielded diverse results, possibly complicated by the influence of the bar. Grosbøl & Carraro (2018) compared the

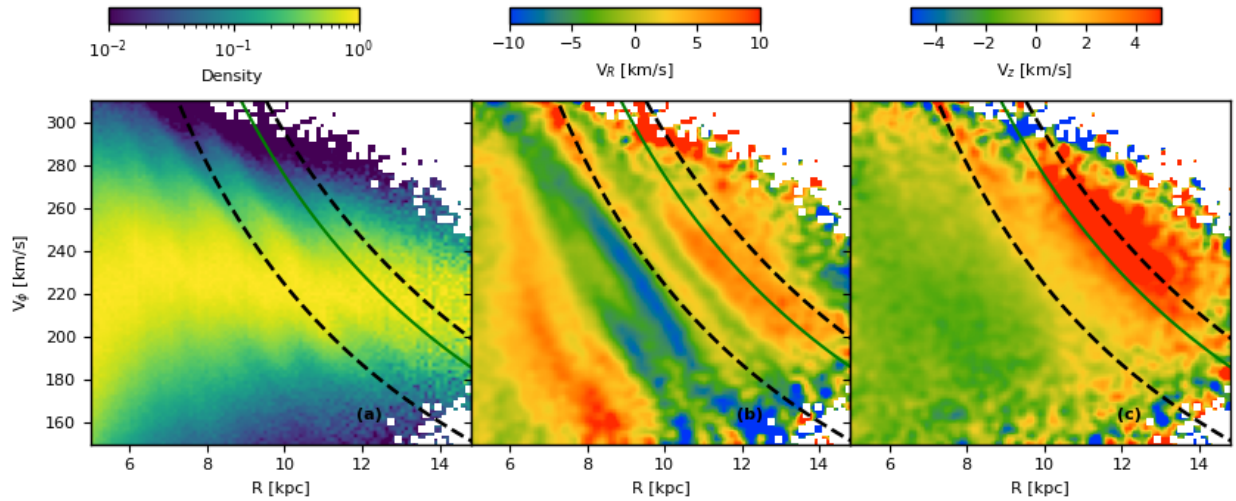

Fig. 8. The RGB sample shown in the $V_\phi - R$ space in density (*panel a*), median V_R (*panel b*), and median V_Z (*panel c*). The two black dotted lines are the locations of the expected OLR and the 1:1 resonance of the Galactic bar. The green solid line marks the location of the discontinuity seen in AC21 and MC22.

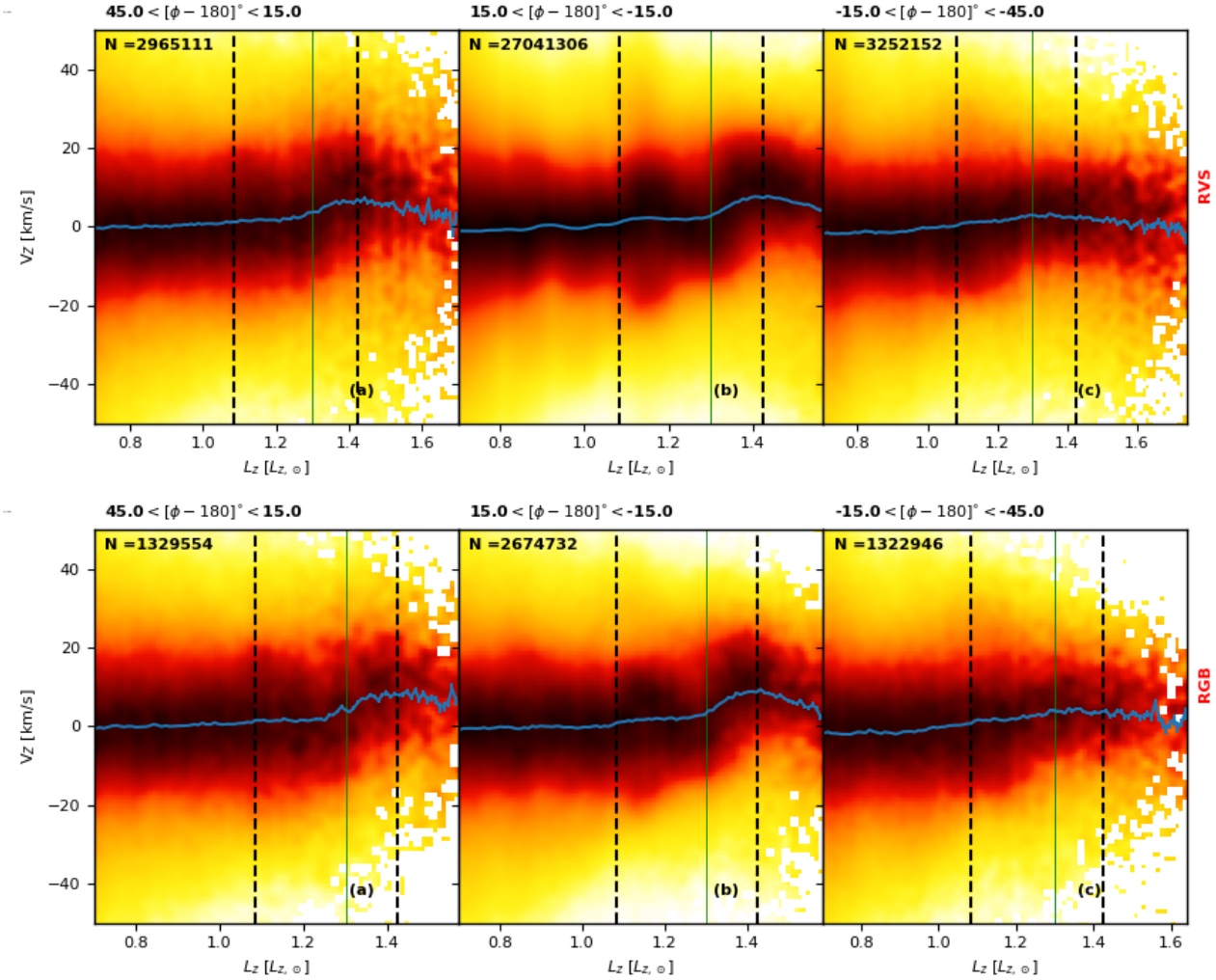

Fig. 9. Distribution of the RV and RGB samples in vertical velocity V_Z against L_Z. The panels divide the data into three bins of 30° width in the azimuth angle, which increases in the direction of Galactic rotation. The middle panel covers stars about 15° either way of the Galactic anticentre. Two dashed black lines are plotted at the positions of the OLR (1.08 $L_{Z,\odot}$), and at the Cepheid gap (1.424 $L_{Z,\odot}$) in Fig. 2. The vertical green line marks the discontinuity (1.3 $L_{Z,\odot}$) noted in recent papers (Gaia Collaboration 2021b; McMillan et al. 2022).

kinematics of young stars as far as 5 kpc from the Sun to simulations and found a range of possible pattern speeds between 20 and 30 km s^{-1} kpc^{-1}. More recently, Monteiro et al. (2021) used a sample of young open clusters and deduced a common pattern speed of 28 km s^{-1} kpc^{-1} from four spiral arm segments, supporting the idea of a long-lived spiral pattern. However, Castro-Ginard et al. (2021) used the same method and a very similar sample of open clusters to arrive at a completely different conclusion, finding different pattern speeds for multiple arm segments. This suggests that the Milky Way spiral arms may be transient, as was also suggested by the study of Quillen et al. (2018), who associated kinematic features in a sample of nearby stars to spiral arm crossings.

Another possibility to be considered is that we see a transient feature from a recent interaction. In their analytic model of a disc-crossing satellite, Binney & Schönrich (2018) showed how the impact of Sgr sets up a large-scale $m = 1$ mode in the outer stellar disc. Interestingly, a hole is punched into the disc at the point of transit owing to the in-plane and vertical deflection of local stars. Bland-Hawthorn & Tepper-García (2021) confirmed this behaviour for the first time in an N-body simulation (their Fig. 7), and showed how the hole is sheared into a strong stellar underdensity at or near the impact radius, here assumed to be 20 kpc. The deep gap occurs between the spiral arms generated by the interaction as they wind up slowly after the event, but the depth of the transition is slowly filled in by orbit migration. This gap remains for a few rotation periods and could reasonably account for what is seen here. However, essentially all Sgr orbit studies to date indicate that the disc transit occurred much farther out than the observed Cepheid gap (e.g. Laporte et al. 2019).

Gaia continues to reveal a surprising amount of structure in the phase space of stars. With each data release, the coverage of the Milky Way disc increases, which has led to the discovery of new kinematic features at each step. The improved quality of the *Gaia* data across the disc allows for a better discrimination between the non-axisymmetric features responsible for resonances, and potentially to distinguish them from transient features that are excited by satellite interactions, which should show significant variation at different azimuthal angles. From the *Gaia* DR3 treasure trove, we have found yet another piece of the Galactic puzzle, one that may help us to identify and disentangle the various dynamical processes shaping the disc of the Milky Way.

Acknowledgements. We thank the anonymous referee for their comments and suggestions. R.D. thanks Ortwin Gerhard for useful discussions. S.K. acknowledges Tomás Ruiz-Lara and Eduardo Balbinot for preparations of the extended radial velocity catalogue, and Eugene Vasiliev for useful discussion on actions. R.D., V.R., G.C. and T.M. are supported in part by the Italian Space Agency (ASI) through contract 2018-24-HH.0 and its addendum 2018-24-HH.1-2022 to the National Institute for Astrophysics (INAF). S.K., T.C.G. and A.C.G. acknowledge support from the European Union's Horizon 2020 research and innovation program under grant agreement No. 101004110. R.D. and S.K. acknowledge Ricky Smart and Luciano Nicastro for use of the computing resources under the GLORIA-project, funded by the European Union 7th Framework Programme under grant agreement n. 283783. P.R. acknowledges support from the University of Barcelona, via a Margarita Salas grant (NextGenerationEU). T.T.G. acknowledges partial financial support from the Australian Research Council (ARC) through an Australian Laureate Fellowship awarded to JBH. We acknowledge the use of the National Computational Infrastructure (NCI) which is supported by the Australian Government, and accessed through the Sydney Informatics Hub (SIH) HPC Allocation Scheme 2022 (PI: TTG; CI: JBH). L.C. acknowledges funding from the Chilean Agencia Nacional de Investigación y Desarrollo (ANID) through Fondo Nacional de Desarrollo Científico y Tecnológico (FONDECYT) Regular Project 1210992. This work presents results from the European Space Agency (ESA) space mission *Gaia*. *Gaia* data are being processed by the *Gaia* Data Processing and Analysis Consortium (DPAC). Funding for the DPAC is provided by national institutions, in particular the institutions participating in the *Gaia* MultiLateral Agreement (MLA). The *Gaia* mission website is https://www.cosmos.esa.int/gaia. The *Gaia* archive website is https://archives.esac.esa.int/gaia. This work has used the following software products: TOPCAT, STIL, and STILTS (Taylor 2005, 2006); Matplotlib (Hunter 2007); IPython (Pérez & Granger 2007); Astropy, a community-developed core Python package for Astronomy (Astropy Collaboration 2018); and Pynbody (https://github.com/pynbody/pynbody).

References

Abdurro'uf, Accetta, K., Aerts, C., et al. 2022, ApJS, 259, 35
Antoja, T., Helmi, A., Romero-Gómez, M., et al. 2018, Nature, 561, 360
Antoja, T., Ramos, P., López-Guitart, F., et al. 2022, A&A, 668, A61
Astropy Collaboration (Price-Whelan, A., et al.) 2018, AJ, 156, 123
Athanassoula, E. 2003, MNRAS, 341, 1179
Babusiaux, C., Fabricius, C., Khanna, S., et al. 2022, A&A, in press https://doi.org/10.1051/0004-6361/202243790
Bailer-Jones, C. A. L., Rybizki, J., Fouesneau, M., Demleitner, M., & Andrae, R. 2021, AJ, 161, 147
Barros, D. A., Lépine, J. R. D., & Junqueira, T. C. 2013, MNRAS, 435, 2299
Bernet, M., Ramos, P., Antoja, T., et al. 2022, A&A, 667, A116
Binney, J. 2012, MNRAS, 426, 1324
Binney, J. 2020, MNRAS, 495, 886
Binney, J., & Schönrich, R. 2018, MNRAS, 481, 1501
Binney, J., & Tremaine, S. 2008, Galactic Dynamics: Second Edition (Princeton: Princeton University Press)
Bland-Hawthorn, J., & Tepper-García, T. 2021, MNRAS, 504, 3168
Bland-Hawthorn, J., Krumholz, M. R., & Freeman, K. 2010, ApJ, 713, 166
Bland-Hawthorn, J., Sharma, S., Tepper-Garcia, T., et al. 2019, MNRAS, 486, 1167
Bovy, J. 2015, ApJS, 216, 29
Bovy, J., Bird, J. C., García Pérez, A. E., et al. 2015, ApJ, 800, 83
Buder, S., Sharma, S., Kos, J., et al. 2021, MNRAS, 506, 150
Carlin, J. L., DeLaunay, J., Newberg, H. J., et al. 2013, ApJ, 777, L5
Castro-Ginard, A., McMillan, P. J., Luri, X., et al. 2021, A&A, 652, A162
Cautun, M., Benítez-Llambay, A., Deason, A. J., et al. 2020, MNRAS, 494, 4291
Cui, X.-Q., Zhao, Y.-H., Chu, Y.-Q., et al. 2012, RAA, 12, 1197
de Zeeuw, T. 1985, MNRAS, 216, 273
Dehnen, W. 2000, AJ, 119, 800
D'Onghia, E., Aguerri, L., & J. A., 2020, ApJ, 890, 117
Fragkoudi, F., Katz, D., Trick, W., et al. 2019, MNRAS, 488, 3324
Gaia Collaboration (Brown, A. G. A., et al.) 2016, A&A, 595, A2
Gaia Collaboration (Katz, D., et al.) 2018, A&A, 616, A11
Gaia Collaboration (Brown, A. G. A., et al.) 2021a, A&A, 649, A1
Gaia Collaboration (Antoja, T., et al.) 2021b, A&A, 649, A8
Gaia Collaboration (Vallenari, A., et al.) 2022a, ArXiv e-prints [arXiv:2208.00211]
Gaia Collaboration (Drimmel, R., et al.) 2022b, A&A, in press https://doi.org/10.1051/0004-6361/202243797
Gaia Collaboration (Recio-Blanco, A., et al.) 2022c, A&A, in press https://doi.org/10.1051/0004-6361/202243511
GRAVITY Collaboration (Abuter, R., et al.) 2021, A&A, 647, A59
Grosbøl, P., & Carraro, G. 2018, A&A, 619, A50
Hunt, J. A. S., & Bovy, J. 2018, MNRAS, 477, 3945
Hunt, J. A. S., Bub, M. W., Bovy, J., et al. 2019, MNRAS, 490, 1026
Hunt, J. A. S., Price-Whelan, A. M., Johnston, K. V., & Darragh-Ford, E. 2022, MNRAS, 516, L7
Hunter, J. D. 2007, Comput. Sci. Eng., 9, 90
Kalnajs, A. J. 1991, in Dynamics of Disc Galaxies, ed. B. Sundelius, 323
Kataria, S. K., & Das, M. 2019, ApJ, 886, 43
Khanna, S., Sharma, S., Bland-Hawthorn, J., et al. 2019a, MNRAS, 482, 4215
Khanna, S., Sharma, S., Tepper-Garcia, T., et al. 2019b, MNRAS, 489, 4962
Khanna, S., Sharma, S., Bland-Hawthorn, J., & Hayden, M. 2022, MNRAS, submitted [arXiv:2204.13672]
Khoperskov, S., & Gerhard, O. 2022, A&A, 663, A38
Laporte, C. F. P., Minchev, I., Johnston, K. V., & Gómez, F. A. 2019, MNRAS, 485, 3134
Levine, E. S., Blitz, L., & Heiles, C. 2006, Science, 312, 1773
Li, Z.-Y. 2021, ApJ, 911, 107
Liu, C., Fu, J., Shi, J., et al. 2020, RAA, submitted [arXiv:2005.07210]
Lucchini, S., Pellett, E., D'Onghia, E., & Aguerri, J. A. L. 2022, MNRAS, 519, 432
Mackereth, J. T., Bovy, J., Leung, H. W., et al. 2019, MNRAS, 489, 176
Malhan, K., Ibata, R. A., Sharma, S., et al. 2022, ApJ, 926, 107
Martinez-Medina, L., Pichardo, B., Peimbert, A., & Valenzuela, O. 2019, MNRAS, 485, L104
McMillan, P. J. 2017, MNRAS, 465, 76

McMillan, P. J., Petersson, J., Tepper-Garcia, T., et al. 2022, MNRAS, 516, 4988
Monari, G., Famaey, B., Siebert, A., Wegg, C., & Gerhard, O. 2019, A&A, 626, A41
Monteiro, H., Barros, D. A., Dias, W. S., & Lépine, J. R. D. 2021, Front. Astron. Space Sci., 8, 62
Mróz, P., Udalski, A., Skowron, D. M., et al. 2019, ApJ, 870, L10
Pedregosa, F., Varoquaux, G., Gramfort, A., et al. 2011, J. Mach. Learn. Res., 12, 2825
Pérez, F., & Granger, B. E. 2007, Comput. Sci. Eng., 9, 21
Pérez-Villegas, A., Portail, M., Wegg, C., & Gerhard, O. 2017, ApJ, 840, L2
Pettitt, A. R., Ragan, S. E., & Smith, M. C. 2020, MNRAS, 491, 2162
Poggio, E., Drimmel, R., Lattanzi, M. G., et al. 2018, MNRAS, 481, L21
Poggio, E., Drimmel, R., Cantat-Gaudin, T., et al. 2021, A&A, 651, A104
Quillen, A. C., Carrillo, I., Anders, F., et al. 2018, MNRAS, 480, 3132
Ramos, P., Antoja, T., & Figueras, F. 2018, A&A, 619, A72
Reid, M. J., & Brunthaler, A. 2020, ApJ, 892, 39
Ripepi, V., Molinaro, R., Musella, I., et al. 2019, A&A, 625, A14
Ripepi, V., Catanzaro, G., Clementini, G., et al. 2022a, A&A, 659, A167
Ripepi, V., Clementini, G., Molinaro, R., et al. 2022b, A&A, in press https://doi.org/10.1051/0004-6361/202243990
Sanders, J. L., & Binney, J. 2016, MNRAS, 457, 2107
Scott, D. W. 1992, Multivariate Density Estimation: Theory, Practice, and Visualization (New York: John Wiley & Sons, Inc.)
Sellwood, J. A. 2010, MNRAS, 409, 145
Skowron, D. M., Skowron, J., Mróz, P., et al. 2019, Science, 365, 478
Steinmetz, M., Matijevič, G., Enke, H., et al. 2020, AJ, 160, 82
Taylor, M. B. 2005, in Astronomical Data Analysis Software and Systems XIV, eds. P. Shopbell, M. Britton, & R. Ebert, ASP Conf. Ser., 347, 29
Taylor, M. B. 2006, in Astronomical Data Analysis Software and Systems XV, eds. C. Gabriel, C. Arviset, D. Ponz, & S. Enrique, ASP Conf. Ser., 351, 666
Tepper-Garcia, T., Bland-Hawthorn, J., Vasiliev, E., et al. 2021, ArXiv e-prints [arXiv:2111.05466]
Tepper-García, T., Bland-Hawthorn, J., & Freeman, K. 2022, MNRAS, 515, 5951
Thomas, G. F., Laporte, C. F. P., McConnachie, A. W., et al. 2019, MNRAS, 483, 3119
Ting, Y.-S., & Rix, H.-W. 2019, ApJ, 878, 21
Trick, W. H. 2022, MNRAS, 509, 844
Trick, W. H., Coronado, J., & Rix, H.-W. 2019, MNRAS, 484, 3291
Trick, W. H., Fragkoudi, F., Hunt, J. A. S., Mackereth, J. T., & White, S. D. M. 2021, MNRAS, 500, 2645
Vasiliev, E. 2019, MNRAS, 482, 1525
Weinberg, M. D. 1994, ApJ, 420, 597
Widrow, L. M., Gardner, S., Yanny, B., Dodelson, S., & Chen, H.-Y. 2012, ApJ, 750, L41
Williams, M. E. K., Steinmetz, M., Binney, J., et al. 2013, MNRAS, 436, 101
Xu, Y., Newberg, H. J., Carlin, J. L., et al. 2015, ApJ, 801, 105
Xu, Y., Liu, C., Tian, H., et al. 2020, ApJ, 905, 6
Yanny, B., & Gardner, S. 2013, ApJ, 777, 91

Appendix A: Results from gas-dynamical simulations

Since classical Cepheid variable stars (Skowron et al. 2019) are mostly younger than the rotation period at the solar circle (220 Myr), it is reasonable to assume that their distribution in phase space reflects the densest gas in the Galactic disc. Most of these will form in star clusters that disperse on the timescale of the disc rotation (Bland-Hawthorn et al. 2010). The unbinding of the clusters injects about $\lesssim$5 km s^{-1} of random motion into the phase-space distribution (Mróz et al. 2019), well within the measurement uncertainty. Therefore, the Cepheid gap can in principle reflect conditions in the gas from which these stars formed.

In order to investigate whether a bar or spiral arm resonance could lead to a similar gap in the distribution of gas in the disc, we ran a gas-dynamical N-body simulation of a Milky Way barred surrogate. In brief, we approximated the Galaxy by a four-component model consisting of a dark matter halo, a stellar bulge, a stellar disc, and a cold (10^3 K), light ($\sim 4 \times 10^9\ M_\odot$) gas disc. The setup of the collisionless components is identical to the model discussed in Tepper-Garcia et al. (2021). The setup of the gas disc follows (Tepper-García et al. 2022). More details about this model will be provided elsewhere (Tepper-García et al., in prep.).

By virtue of the disc-to-total mass ratio of the model, the disc is subject to a bar instability. A bar forms after about 2.5 Gyr of evolution in isolation, and remains reasonably stable for at least another 1.5 Gyr.

To estimate the bar pattern speed Ω_p, which dictates the location of the relevant resonances, we relied on a Fourier analysis of the surface density of the stellar disc. In brief, we calculated the amplitude (A_2) and the phase (ϕ_2) of the $m = 2$ mode in a specified radial range ($R \leq 10$ kpc), and computed the phase change ($\dot{\phi}_2$) for the datum at which A_2 reaches a maximum, consistent with the estimate of the bar strength (e.g. Kataria & Das 2019). As a check, we calculated both a pure arithmetic mean of and a radially weighted average of $\dot{\phi}_2$ over the specified radial range (e.g. Athanassoula 2003). Each of these approaches yields a slightly different value (see the discussion in Tepper-Garcia et al. 2021), but they are all consistent with $\Omega_p \approx 30-40$ km s^{-1} kpc^{-1} for the bar at $T \approx 1.5$ Gyr after its formation.

At this epoch, we studied the distribution of gas in the synthetic galaxy at $T \approx 4$ Gyr (Fig. A.1). We divided the volume occupied by the disc (i.e. the volume enclosed by $R = 20$ kpc and $|z| = 5$ kpc) into four quadrants, where quadrant 1 was defined by the region enclosed by $0 \leq \phi < 90$, quadrant 2 by $90 \leq \phi < 180$, and so on (where ϕ is the azimuthal angle), and analysed the distribution of gas in each of the quadrants in $R - V_\phi$ space, that is, the rotation curve. The intent was to determine whether the gas angular momentum (L_Z) undergoes any discontinuities, for instance from disc resonances, gas compression, or shocks. The result of this exercise is shown in Fig. A.2. In brief, none of the panels displays a clear gap in the distribution of gas, as seen in the rotation curve of the Cepheid population (Fig. 1, left panel).

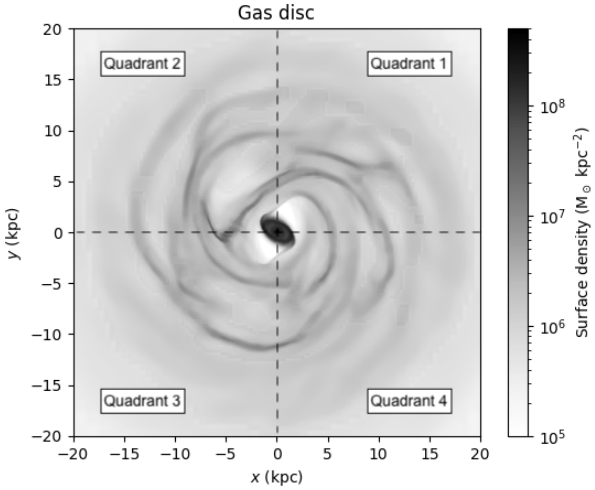

Fig. A.1. Distribution of gas in a Milky Way surrogate 1 Gyr after the formation of the central bar. For the purpose of the analysis, we divided the disc face into four quadrants identified by the numbers 1 through 4, as indicated in the figure. See also Fig. A.2.

There may be several reasons for the disagreement. The most obvious is our assumption that the dense gas in a thin 2D plane is an appropriate proxy for the Cepheid distribution. This is the most favourable situation for strong resonances to operate. However, the resonances must then set up on a very short timescale, that is, in less than one rotation period, and this is not easy to do.

Furthermore, it has long been known that the gas disc is corrugated with a wave amplitude of roughly 300 pc (see references in Tepper-García et al. 2022). The phase-spiral effect is dominated by the younger stars (Bland-Hawthorn et al. 2019). Another possibility is that the observed gap is transient, except that we produced a movie of the quadrant rotation curves, and no gaps were seen for one billion years after the bar formed. This needs to be revisited with higher-resolution simulations.

Finally, it is possible that the gap is not triggered by the bar, and thus our isolated model is not able to reproduce it. This idea is supported by the fact that other recently discovered kinematic features in the Galaxy such as the phase spiral or the 11 kpc break reported by AC21 are likely the result from a strong impulsive interaction (e.g. Bland-Hawthorn & Tepper-García 2021; McMillan et al. 2022).

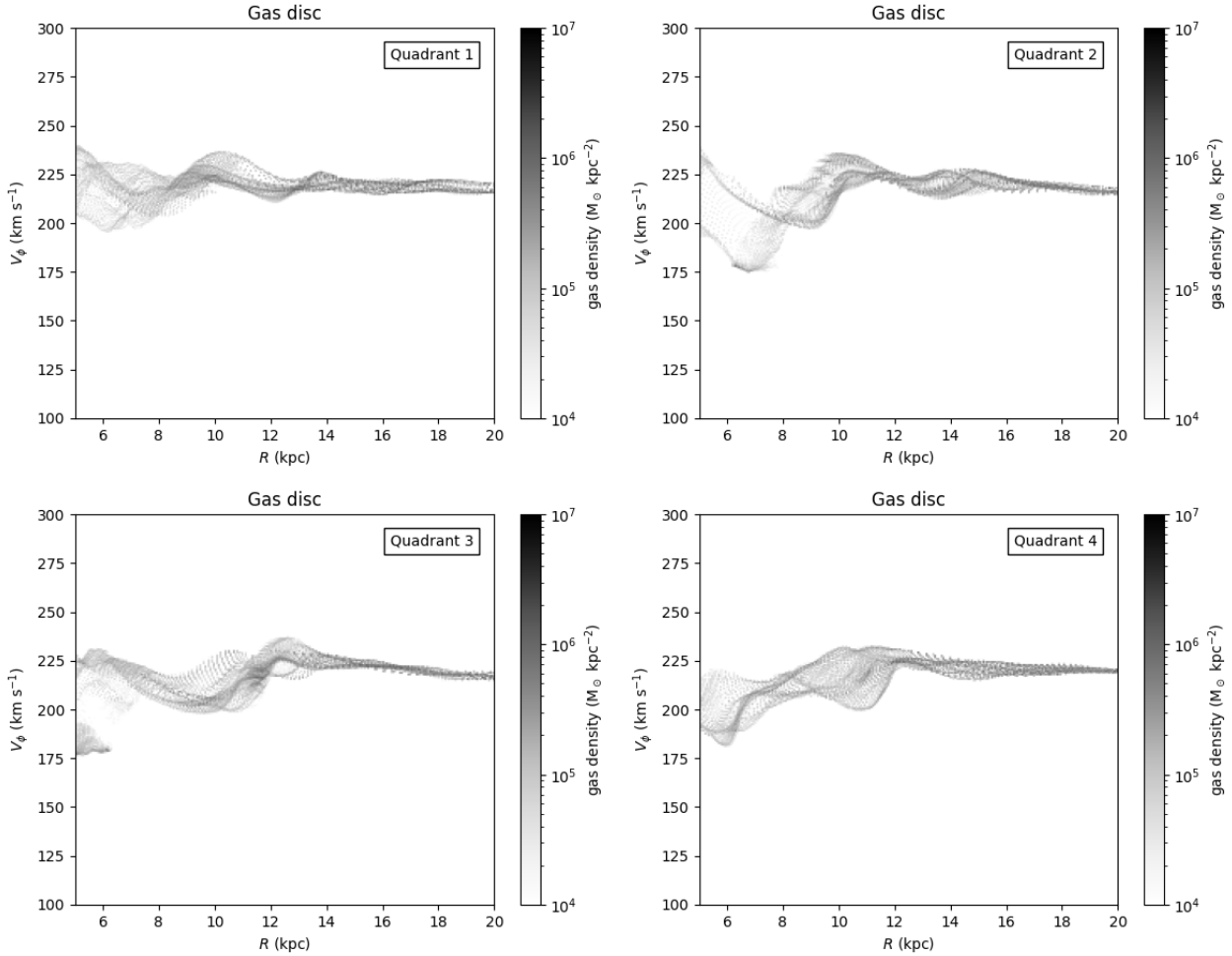

Fig. A.2. Rotation curve of the gas in each of the quadrants displayed in Fig. A.1 weighted by gas density. No gap is apparent in any of the panels. See text for more details.